JBIC (1999) 4:209–219

ORIGINAL ARTICLE

Sandra Macedo-Ribeiro · Wieger Hemrika
Rokus Renirie · Ron Wever · Albrecht Messerschmidt

X-ray crystal structures of active site mutants of the vanadium-containing chloroperoxidase from the fungus *Curvularia inaequalis*

Received: 12 October 1998 / Accepted: 25 January 1999

Abstract The X-ray structures of the chloroperoxidase from *Curvularia inaequalis*, heterologously expressed in *Saccharomyces cerevisiae*, have been determined both in its apo and in its holo forms at 1.66 and 2.11 Å resolution, respectively. The crystal structures reveal that the overall structure of this enzyme remains nearly unaltered, particularly at the metal binding site. At the active site of the apo-chloroperoxidase structure a clearly defined sulfate ion was found, partially stabilised through electrostatic interactions and hydrogen bonds with positively charged residues involved in the interactions with the vanadate in the native protein. The vanadate binding pocket seems to form a very rigid frame stabilising oxyanion binding. The rigidity of this active site matrix is the result of a large number of hydrogen bonding interactions involving side chains and the main chain of residues lining the active site. The structures of single site mutants to alanine of the catalytic residue His404 and the vanadium protein ligand His496 have also been analysed. Additionally we determined the structural effects of mutations to alanine of residue Arg360, directly involved in the compensation of the negative charge of the vanadate group, and of residue Asp292 involved in forming a salt bridge with Arg490 which also interacts with the vanadate. The enzymatic chlorinating activity is drastically reduced to approximately 1% in mutants D292A, H404A and H496A. The structures of the mutants confirm the view of the active site of this chloroperoxidase as a rigid matrix providing an oxyanion binding site. No large changes are observed at the active site for any of the analysed mutants. The empty space left by replacement of large side chains by alanines is usually occupied by a new solvent molecule which partially replaces the hydrogen bonding interactions to the vanadate. The new solvent molecules additionally replace part of the interactions the mutated side chains were making to other residues lining the active site frame. When this is not possible, another side chain in the proximity of the mutated residue moves in order to satisfy the hydrogen bonding potential of the residues located at the active site frame.

Key words Sulfate binding · Mutants · Phosphate · Chloroperoxidase · Vanadate

Abbreviations *CPO* vanadium-containing chloroperoxidase from *Curvularia inaequalis* · *APO* recombinant apo-chloroperoxidase · *HOLO* recombinant chloroperoxidase reconstituted with vanadate · *H404A* mutant of CPO where histidine 404 was replaced by an alanine · *H496A* mutant of CPO where histidine 496 was replaced by an alanine · *D292A* mutant of CPO where aspartate 292 was replaced by an alanine · *R360A* mutant of CPO where arginine 360 was replaced by an alanine · *Sol* solvent water molecule

Introduction

Haloperoxidases are enzymes which catalyse, in the presence of hydrogen peroxide, the oxidation of halides (iodide, bromide and chloride) to their corresponding hypohalous acids:

$$H_2O_2 + H^+ + X^- \rightarrow H_2O + HOX$$

A diverse number of halogenated substrates can subsequently be generated if the appropriate nucleophilic acceptors are present. Three classes of haloperoxidases

S. Macedo-Ribeiro · A. Messerschmidt (✉)
Max-Planck Institut für Biochemie
Abteilung Strukturforschung, Am Klopferspitz 18A
D-82152 Martinsried, Germany
e-mail: messersc@biochem.mpg.de
Tel.: +49-89-85782678
Fax: +49-89-85783516

W. Hemrika · R. Renirie · R. Wever
E.C. Slater Institute, Biocentrum, University of Amsterdam
Plantage Muidergracht 12, 1018 TV Amsterdam
The Netherlands

are presently known. One of these has been identified mainly in bacteria and contains no prosthetic group [1, 2]. The remaining two classes comprise the heme-containing haloperoxidases [3, 4] and the vanadium-containing haloperoxidases [5–9]. Vanadium haloperoxidases bind a vanadate ion as a prosthetic group and include the vanadium bromoperoxidases, mainly found in marine algae, and the vanadium chloroperoxidases, mainly isolated from terrestrial fungi.

The chloroperoxidase (CPO) secreted by the fungus *Curvularia inaequalis* [10] is a vanadium enzyme which is involved in the production of hypochlorous acid (HOCl). HOCl is a strong bactericidal agent which may oxidise plant cell walls [11], thus facilitating the pathogenic role of the fungi. This enzyme is largely thermo- and chemostable, resisting to temperatures up to 70 °C and to oxidative inactivation in the presence of high concentrations of peroxide. The crystal structure of native CPO, a 67 kDa protein, has been determined to 2.03 Å resolution. It shows 2 four-helix bundles as the main structural motifs [12, 13]. These helical structures have been proposed to be the major structural elements of the protein, providing a strong stabilising hydrophobic effect. The vanadium binding site is located at the top of the C-terminal second four-helix bundle. The vanadium coordination geometry is trigonal bipyramidal with three oxygen atoms in the equatorial plane (bond lengths about 1.65 Å), one apical oxygen atom (bond length 1.93 Å) and the other apical nitrogen atom from His496 (bond length 1.96 Å). The negative charge is compensated by hydrogen bonding interactions with positively charged or hydrophilic residues located at the active site. Residues Lys353, Arg360, Ser402, Gly403 and Arg490 form hydrogen bonds with the equatorial non-protein oxygens of vanadate. Each of the three equatorial oxygen atoms is hydrogen bonded with at least one positively charged function, which means that these oxygen atoms are deprotonated. The apical oxygen ligand has a bond length (1.93 Å) which is in the range of a V(V)-hydroxyl bond and it is hydrogen bonded to nitrogen Nδ1 of His404. This residue was proposed to function as the acid-base group in catalysis [12]. It has been shown [14] that binding of hydrogen peroxide is inhibited when a group of pK_a larger than 5 is protonated. Thus, in the active protein, the apical hydroxyl group is the H-donor and the nitrogen Nδ1 of His404 is the H-acceptor of the hydrogen bond. This residue was proposed to function as the acid-base group in catalysis.

Sequence alignment between this vanadium chloroperoxidase and the vanadium-containing bromoperoxidase from *Ascophyllum nodosum* [7], an enzyme which is believed to have a similar catalytic mechanism [14], revealed high similarities in the metal binding site, but very low similarities in the remaining regions. Surprisingly, those stretches of the sequence were also found to be present in three families of acid phosphatases, indicating similarities in the anion-binding active sites of all these enzymes [15, 16]. Furthermore, studies with the apo-CPO produced recombinantly showed that it can also function as an acid phosphatase, supporting the hypothesis for the common architecture of the active sites from these enzymes [15].

In order to further analyse the putative structural implications of the active site residues in cofactor binding and peroxidase activity, we have determined the crystal structure of active site mutants of CPO. Further, a correlation is made with the available preliminary kinetic data obtained for each of these mutants. Furthermore, we obtained data and solved the structure of the recombinant apo-chloroperoxidase (APO) at 1.66 Å resolution and determined the crystal structure of recombinant chloroperoxidase reconstituted with vanadate (HOLO).

Materials and methods

Activity measurements and mutants

Enzyme activity was determined by measuring the chlorination of monochlorodimedon ($E = 20.2\ nM^{-1}.cm^{-1}$ at 290 nm). The reaction mixture contained 50 mM citrate (pH 5.0), 5 mM NaCl, 1 mM H_2O_2 and 100 mM sodium vanadate. A detailed description of the procedures to construct the mutants and their expression will be published elsewhere.

Crystallisation and data collection

Recombinant apo-chloroperoxidase (APO) and mutants of CPO (D292A, H496A, H404A and R360A) were produced in a *Saccharomyces cerevisiae* expression system as described previously [15]. The recombinant material tends to form crystalline precipitates when the crystallisation conditions determined for the native crystals are used [13]. Thus, the crystallisation conditions were altered in order to allow for slower equilibration rates. The crystals from the recombinant material take 2–3 months to grow. Crystals of D292A, H496A, R360A and recombinant holoenzyme (HOLO) grew at 4 °C by vapour diffusion. Hanging drops were made from 3 µl of protein solution [5 mg/ml in 5 mM MOPS (3-morpholinopropanesulfonic acid) (pH 7.5), 1 mM vanadate], 3 µl of precipitating buffer containing 1.7 M ammonium sulfate, 0.1 M Tris-H_2SO_4 (pH 8.0), 1 mM sodium vanadate and 0.3 µl 0.1 M *l*-cysteine. Crystals from APO were prepared in a similar way from a precipitating buffer without sodium vanadate. The material from the mutant H404A was largely insoluble when added to the crystallisation buffer mentioned above. Thus, crystals from H404A were obtained from 1.3 M ammonium sulfate, 0.1 M Tris-H_2SO_4 (pH 8.0) at 20 °C, after microseeding pre-equilibrated protein drops with native protein crystals [13]. For the crystallisation of the recombinant material it was always necessary to induce crystal nucleation. This was the main reason for the inclusion of *l*-cysteine as an additive, which crystallises as hexagonal plates in the crystallisation conditions used. All crystals belong to space group *R*3 and all but the crystals from the mutant H404/A are isomorphous with the native enzyme crystals. The H404A mutant crystals have a smaller unit cell when compared with the native protein crystals.

Room temperature diffraction data were collected on a Hendrix/Lenfter X-ray image-plate system (Mar-Research, Hamburg, Germany) mounted on a Rikagu rotating anode generator operating at 5.4 kW ($\lambda Cu_{K\alpha} = 1.5418$ Å). Cryo data were collected from a flash-cooled APO crystal [15% glycerol, 2.6 M ammonium sulfate, 0.15 M Tris-H_2SO_4 (pH 8.0) on the wiggler beamline BW6 at DORIS (DESY, Hamburg). Data were processed with

Table 1 Data collection and refinement statistics

Parameter	H404 A	D292 A	H496 A	APO	HOLO	R360 A
Crystal parameters						
Space group	R3	R3	R3	R3	R3	R3
Unit cell constants						
$a=b$ (Å)	129.60	131.96	131.34	130.04	131.84	131.64
c (Å)	104.45	112.90	112.66	112.15	112.83	112.85
α (°)	90	90	90	90	90	90
β (°)	90	90	90	90	90	90
γ (°)	120	120	120	120	120	120
Diffraction data						
Resolution[a] (Å)	2.20/ 2.20–2.26	2.15/ 2.15–2.27	2.11/ 2.11–2.16	1.66/ 1.66–1.69	2.15/ 2.15–2.27	2.35/ 2.35–2.48
Total observations	249169	326397	112709	430434	164218	267056
No. of unique observations	33094	39193	40714	81916	39327	30310
Completeness[a] (%)	99.6/100	98.3/100	97.6/75.6	99.0/99.0	99.2/95.6	99.8/99.8
R_{merge}[a,b] (%)	10.3/47.5	8.2/37.7	8.7/44.7	6.9/33.9	6.9/27.8	9.7/39.0
Multiplicity	3.1	3.7	3.2	3.1	2.7	3.2
I/SIGI[a]	7.0/1.6	7.0/1.9	7.0/0.6	7.0/2.3	6.2/2.4	5.7/1.8
Refinement						
Resolution range (Å)	8.0–2.20	8.0–2.15	8.0–2.11	8.0–1.66	8.0–2.15	8.0–2.35
No. of reflections in this range	32533	38577	39954	81244	38638	29585
R[a,c] (%)	18.2/27.2	17.9/26.0	18.8/32.5	17.9/34.3	18.1/25.8	18.8/32.5
R_{free}[a,d]	21.3/24.8	21.7/30.2	21.9/37.2	21.6/32.1	22.6/24.3	22.8/32.4
Mean coordinate error (Å)[e]	0.23	0.22	0.24	0.19	0.23	0.21
σ of mean coordinate error (Å)[e]	0.01	0.01	0.02	0.02	0.01	0.02
No. of atoms						
All non-hydrogen atoms	4700	4754	4744	5031	4739	4715
Non-hydrogen protein atoms	4479	4481	4479	4484	4484	4478
Solvent	216	268	260	537	250	232
Ligand	5 (VO_4)	5 (VO_4)	5 (VO_4)	2×5 (SO_4)[f]	5 (VO_4)	5 (VO_4)
Average temperature factor (Å^2)						
All atoms	24.90	27.13	29.82	26.23	31.22	30.86
Protein atoms	24.46	26.55	29.27	24.91	30.71	30.38
Solvent	33.85	37.02	39.07	36.92	40.51	40.11
Ligand	21.60	16.19	37.50	24.66/58.88[f]	20.90	28.20
R.m.s. deviation for bonded B values (Å^2)	1.89	2.01	1.72	1.62	1.84	1.95
R.m.s deviations from standard geometries						
Bonds (Å)	0.006	0.006	0.006	0.007	0.006	0.008
Angles (°)	1.504	1.511	1.615	1.673	1.574	1.511
Protein Data Bank (PDB) accession codes	1vng	1vne	1vnh	1vns	1vni	1vnf

[a] Overall/outer shell

[b] $R_{merge}=\Sigma\Sigma/I(h)_I-<I(h)>|/\Sigma\Sigma I(h)_I$, where $I(h)_I$ is the observed intensity of the ith source and $<I(h)>$ is the mean intensity of reflection h over all measurements of $I(h)$

[c] $R=\Sigma(F_o-F_c)/\Sigma F_c$

[d] R_{free} is the cross-validation R-factor computed for the test set of reflections (5% of total number of reflections) which were omitted in the refinement process

[e] Determined from Luzzati plot

[f] Two sulfates were built into this APO structure. The first number represents the sulfate found at the active site and the second corresponds to a sulfate localised at the protein surface

MOSFLM [17] and programs from the CCP4 suite [18]. Crystal parameters and data collection statistics are depicted in Table 1.

Structure determination and crystallographic refinement

The crystallographic phases of the native enzyme structure[12, 13] were used as the starting phases for the refinement of the APO, HOLO, H496A, D292A and R360A. The initial phases for the H404A model were obtained after molecular replacement with AMoRe [19], using the native protein model [12, 13]. The models were refined with XPLOR [20] using the parameters derived by Engh and Huber [21], and model building was done with TurboFRODO [22]. For all the structures refined the F_{obs} were scaled to the F_{calc} by using overall anisotropic B-factor refinement with XPLOR [20]. The equilibrium bond lengths and angles for the sulfate group were derived from sulfate refined in the crystal structure of rubredoxin [23]. For the determination of the equilibrium bond lengths and angles for the vanadium metal site in each of the structures described, electron density maps were calculated from refined models without vanadate and the vanadium and oxygen atoms were optimally placed in the resulting differ-

ence electron density. For these experimentally determined bond distances and angles, force constants of 1000 and 200 kJ mol^{-1}, respectively, were applied in the energy restrained refinement.

The refinement statistics for the current models are shown in Table 1. In all structures, residues 1–3 and 578–609 were excluded from the models because they were not visible in the electron density and are probably mobile or disordered. Residues 118–127 are also not defined in the electron density and thus their occupancies were set to zero. Additionally for some of the structures, residues 390–395 were not clearly visible in the electron density and the occupancy of their side chains was set to zero. Hydrogen bonds were calculated with HBPLUS [24]. Figures 1, 2 and 4–9 were prepared with SETOR [25]. Figure 3A and B were produced with INSIGHTII (Biosym/MSI) and Fig. 3C and D were prepared with GRASP [26].

Results and discussion

Overall structure

Superpositions of the refined protein models with the native enzyme [13] revealed that, within the error limits of the electron density maps, the overall backbone structure remains unchanged. The root mean square (r.m.s.) deviations of the atomic coordinates between the analysed structures are depicted in Table 2. The mean positional errors, as estimated from the Luzzati plots (Table 1), are around 0.2 Å and are likely to be lower for the well-defined parts of the structure and for the metal binding site.

The residues in the active site are clearly defined in the electron density maps for all models. Alterations in conformation are observed at the surface of mutant H404A. The crystals of this mutant display a smaller cell, particularly a 8 Å shorter *c*-axis. In the H404A model the side chains of residues Arg177 and Glu182 are in a different conformation and do not form a salt bridge as observed in the native protein structure (Fig. 1). The different conformations of these residues alter the crystal contacts, resulting in a smaller crystallographic unit cell and affecting its solubility under high salt conditions. This does not seem to be a direct effect of the mutation of the active site residue His404, which is relatively far from the site where these changes occur. Instead it seems to result from an alteration of the main chain conformation of residues 123 and 124 which are not defined in the electron density of any of the structures.

Residues Asp390-Pro396 are very flexible in the recombinant protein material (as observed from the high *B*-values in this region), although their density was clearly defined in the native protein structure. A similar situation occurs for the protein segment including residues Glu196-Gln220. Residues Asp390-Pro396 form part of the broad channel leading to the anion-binding site. In the native protein structure, Pro395 and Phe393 are in the immediate vicinity of the bound vanadate ion (see Figs. 2, 3A). The side-chain of Lys394 points away from the active site and is fixed by a hydrogen bond with the main-chain carbonyl of Gly494. In the structures of the mutants D292A and R360A, most of these residues are well defined in the electron density map. In the D292A mutant the main chain of residues such as Phe393 deviates more than 7 Å from its original position in the native structure (Figs. 2, 3B) and the side chain of Lys394 is hydrogen bonded to Ala292O. The displacement of the mentioned residues causes small alterations in the conformations of the side chains of Glu196, Phe218 and Gln220. In the APO form of the recombinant protein the well-defined electron density indicates that this region assumes a conformation similar to the native protein. In the R360A mutant the conformation of the region containing residues Asp390-Pro396 is well defined and similar to the native CPO. For the mutants H404A, H496A and for the HOLO form of the recombinant native protein this region is not well defined and it seems that the conformation of this protein stretch is alternating between the two main observed conformations. The movements of this region generate considerable alterations of the electrostatic potential distribution in the vicinity of the active site channel (Fig. 3C, D). The amino acid residues included in these regions are the same present in the native enzyme and the nucleotide sequence in this region has been reconfirmed. Thus the alterations in the conformations of these residues could be a consequence of misfolding of the protein in the *Saccharomyces cerevisiae* expression system. As a result the protein expressed recombinantly is more difficult to crystallise and the crystals obtained have one or the other predominant conformation.

Oxyanion binding site in apo-chloroperoxidase

In the initial difference electron density maps for the recombinant apoenzyme (APO), strong electron density (maximum four times the standard deviation of the difference electron density map, 4σ) was found at the active site. The spherical electron density located close to His496 was too strong to simply represent a bound

Table 2 Average r.m.s.d. values of atomic coordinates (Å)

	HOLO	APO	H404A	D292A	H496A	R360A
NATIVE[13]	0.281	0.309	0.421	0.357	0.256	0.228
HOLO		0.289	0.257	0.151	0.174	0.170
APO			0.379	0.328	0.212	0.233
H404 A				0.247	0.325	0.336
D292 A					0.236	0.260
H496 A						0.127

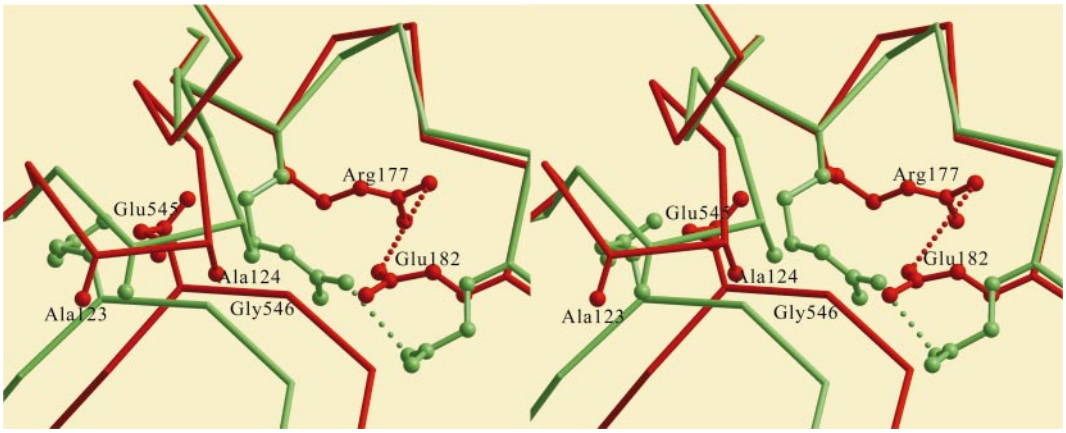

Fig. 1 Movements of the side chain of Arg177 in the mutant H404A alter the crystal contacts with the main chain of residues 545–546 of the symmetry related molecule. Schematic view of the crystal contacts in the H404A mutant (*red*) in comparison to the corresponding region in the native protein structure [13] (*green*)

water molecule as previously modelled into the apo-chloroperoxidase after removal of the vanadium cofactor from the native protein [27]. Because no vanadate was added to the recombinant protein before or during crystallisation, it was assumed that the species bound to the metal cofactor binding site could be a tetrahedral sulfate anion, present in high concentrations in the crystallisation buffer. The presence of a number of positively charged residues, which usually form hydrogen bonds with the vanadate, probably compensate the strong negative charge of the sulfate ion. This hypothesis was further confirmed in the electron density maps calculated with the higher resolution data obtained from frozen apo-CPO crystals. Thus, a tetrahedral sulfate was built into the difference electron density and refined. The final omit map for His496 and the sulfate group close by is displayed in Fig. 4 and shows clearly the density for the bound oxyanion. Figure 4A shows a scheme of the interactions between the sulfate and the active site residues. The sulfur is 2.92 Å away from the Nε2 of His496 and the sulfate is held by hydrogen bonds to the side chains of Lys353 (2.81 Å), Arg490 (3.20 and 3.01 Å), Arg360 (3.01 and 3.24 Å) and Ser402 (2.69 Å) and additionally to the main chain nitrogen atoms of Gly403 (2.80 Å) and His404 (3.19 Å) and to a water molecule (2.53 Å). His496 is positioned by a hydrogen bond to the side chain of Asp500 (2.93 Å). Minor differences are observed in the positions of the amino acid side chains in the sulfate bound form when compared to the native enzyme. Most deviations occur for the side chains of His404, which gets closer to the apical oxygen of the bound oxyanion (2.99 Å), and His496, which moves further away from the sulfate because a covalent bond is no longer formed. Residues His404 and His496 are within hydrogen bonding distances to the sulfate ion as depicted in Fig. 4A. In the absence of the covalently bound vanadate, the sulfate ion could possibly cause a pK_a shift so that both His496

Fig. 2 Stereo view of the main chain and side chain conformational changes in stretch Asp390-Pro396 in mutant D292A (*green*) superimposed with the native protein (*red*). The active site residues displayed in *blue* and labelled in *black* correspond to mutant D292A. The vanadate ion is depicted in *blue*. In the APO protein structure this stretch of residues is similar to the native protein. The same is true for the mutant R360A, where only the conformation of the side chain Lys394 is altered. For the HOLO protein structure and for mutants H404A and H496A this region is not well defined in the electron density and seems to alternate between its conformation in the native protein [13] and in the mutant D292A

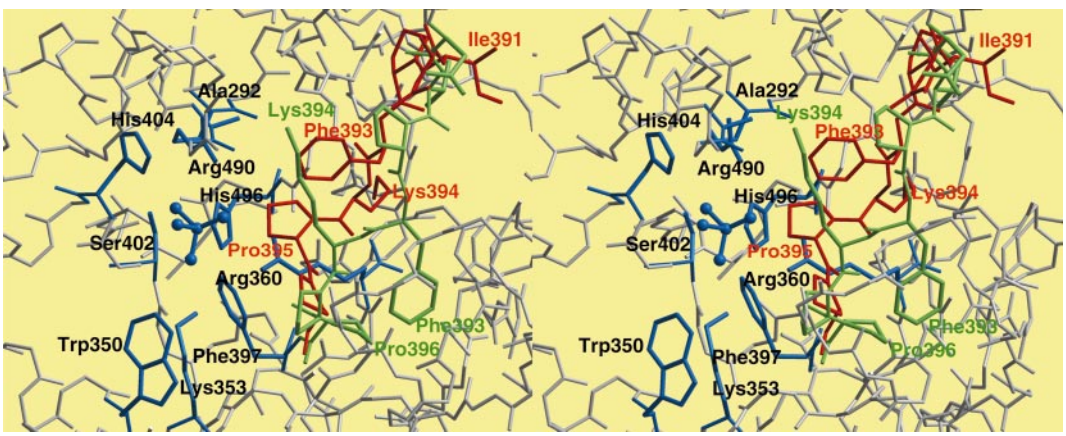

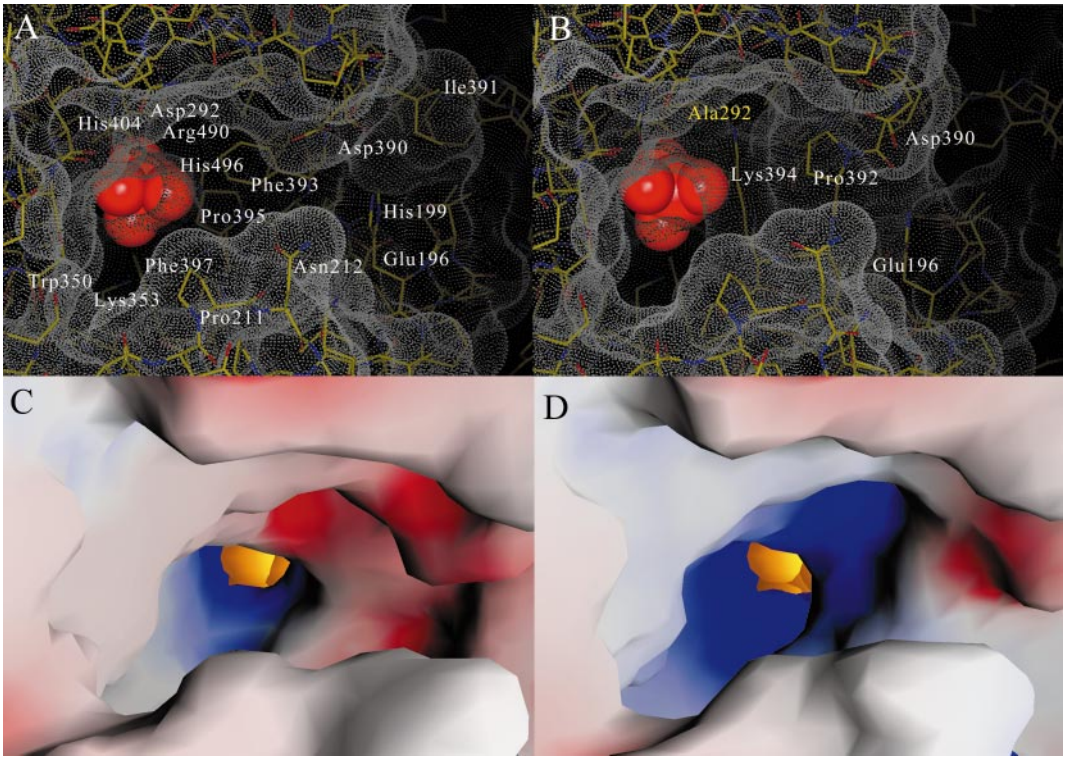

Fig. 3A-D View of the wide channel leading to the active site vanadium. The vanadate is represented as *red* (**A, B**) or as *yellow* spheres (**C, D**). In this view the vanadate binding His496 comes from the right and is protected from the solvent. Ser402 comes from the back of the plane of the figures and Lys353, as well as residues Trp350 and Phe397, are visible at the bottom. Arg360 is located to the right side of the vanadate. His404, in this orientation, is located at the top of the vanadate ion to its left. In frames **A** and **B** the Connolly surface is represented as small *white dots* and the protein as a *stick model* (carbon, *yellow*; oxygen, *red*; nitrogen, *blue*). In frames **C** and **D** the electrostatic potential in the immediate vicinity of active site entrance is displayed from $-15k_BT$ (*red*) to $15k_BT$ (*blue*) (where k_B is the Boltzmann's constant and T is the absolute temperature). In the calculation of the molecular surface and the electrostatic potential, the vanadate was omitted and a salt concentration of 0.145 M was used. In frames **A** and **C** the native protein model [13] is shown for comparison with the D292A mutant (frames **B** and **D**). To the left of the vanadate and to the exterior of the active site a clear difference in the electrostatic potential is visible, resulting partially from the movement of the 390–396 loop

and His404 could become doubly protonated and indeed form additional hydrogen bonds.

The protein seems to form a rigid matrix, allowing the formation of a very well-defined oxyanion binding site as seen previously in the structure of the tungstate-bound CPO [27]. The structure of the recombinant apo-enzyme showed that this active site frame provided by the protein residues remains mainly unchanged. The residues Asp292, Lys353, Arg360, Ser402, Gly403, His404 and Arg490 involved in binding of the vanadate (HVO_4^{2-}) in the native enzyme show only small conformational changes necessary to accommodate an anion with a smaller size and different protonation state (SO_4^{2-}).

The vanadium binding site in the reconstituted chloroperoxidase (HOLO)

The recombinant enzyme reconstituted by addition of sodium vanadate in a final concentration of 1 mM clearly showed the vanadium covalently bound to His496 (1.94 Å) with a trigonal bipyramidal geometry with three equatorial (bond distances around 1.60 Å) and one apical (2.15 Å) non-protein oxygen ligands. The distance to the apical ligand is within the range of a water ligand at this position, according to structural studies with model compounds [28–32]. As observed in Fig. 5B, there is still some extra density above this ligand. The reasons for this extra density are not clear, considering that no chloride was used in the protein preparation and crystallisation. The strong affinity of this enzyme for vanadate, even with the high concentrations of sulfate present, also exclude the possibility that this density could represent a mixture between sulfate and the vanadate at the active site. Several trials to fit into this density different types of ligands such as methoxide or ethoxide did not allow us to explain this electron density unambiguously.

This active site is very similar in conformation and geometry to the active site of the native protein [13]. As previously observed in the native protein structure, the anion binding site provides a rigid matrix stabilised by a number of hydrogen bonds (Fig. 5A). As observed for the native protein, the side chains of the amino acid residues interacting directly with the vanadate are held in an ideal conformation by additional hydrogen bonds with residues in the proximity of the active site (Table 3). A strong salt bridge is also observed between re-

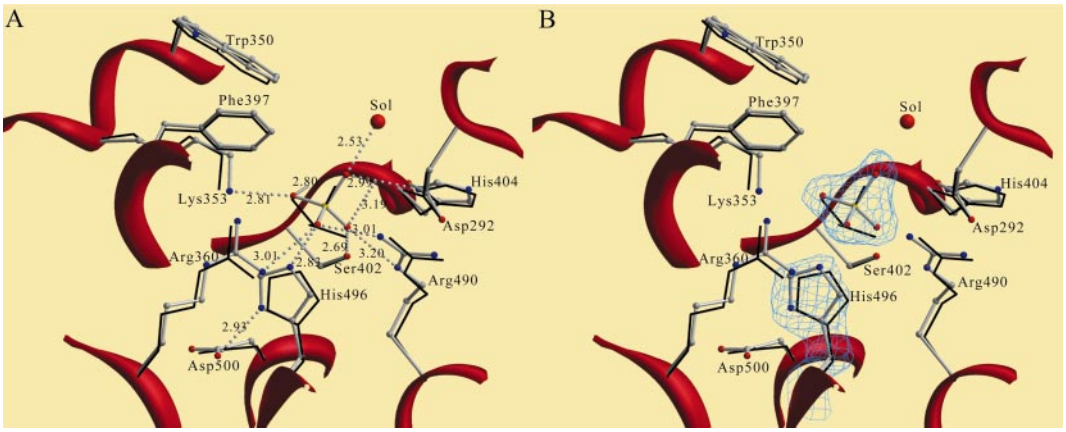

Fig. 4A,B Sulfate interactions at the active site of apo-chloroperoxidase (APO). The sulfate ion is displayed with oxygens in *red* and the sulfur atom in *yellow*. **A** The hydrogen bonds are represented as *grey spheres* and the distances are indicated in Å. **B** The electron density map contoured at 4σ was calculated after omitting His496 and the bound sulfate ion. For comparison the conformation of the same residues in the native protein [13] is displayed in *black*

sidues Asp292 and Arg490 which seems to hold Arg490 in a perfect conformation for a hydrogen bond to the bound vanadate.

H404A

Histidine 404 is proposed to play a crucial role as a general base in catalysis [12]. Steady-state kinetic data indicate that protonation of a residue with a pK_a higher than 5 prevents binding of the peroxide during the catalytic reaction [14]. This residue was proposed to be His404. Hydrogen bonding between H404 and the apical protonated oxygen of the bound metal cofactor is believed to increase the nucleophilicity of the apical hydroxyl group, allowing it to take up a proton from the incoming peroxide and then leave the vanadium coordination sphere as a water molecule.

At the active site, removal of the His404 side chain causes a rupture of the salt bridge between Arg490 and Asp292 (Fig. 6). Arg490 moves into the space originally occupied by the side chain of His404 and makes hydrogen bonds to the carbonyl groups of Ala290 (3.09 Å) and Trp298 (2.79 Å, not shown in Fig. 6A). In the native protein structure a hydrogen bond is observed between His404Nε2 and Trp289O. Close to the vanadium binding site, solvent molecules replace part of the hydrogen bonds to the vanadate oxygens which were disrupted by the large movement of Arg490 side chain. The side chain of Asp292 also moves away from its original position and is only stabilised by a hydrogen bond with one of the new solvent molecules.

At the active site the vanadate ion is found covalently bound to His496 (1.96 Å). The apical oxygen atom is 2.0 Å away from the vanadium as observed in omit maps analysed after the final refinements, possibly corresponding to a mixture between hydroxyl and water ligands at this position [28, 33]. The bond distances between the vanadium and the equatorial oxygen atoms are on average 1.60 Å.

Fig. 5A,B Active site view of HOLO. The vanadate is displayed as a *ball and stick model* with oxygens in *red* and the vanadium atom in *blue*. For comparison the conformation of the same residues in the native protein [13] is displayed in *black*. Part of the main chain is represented as a *red ribbon*. **A** The hydrogen bonds are represented as *grey spheres* and the distances are indicated in Å. **B** The electron density map contoured at 4σ was calculated after omitting His496 and the bound vanadate

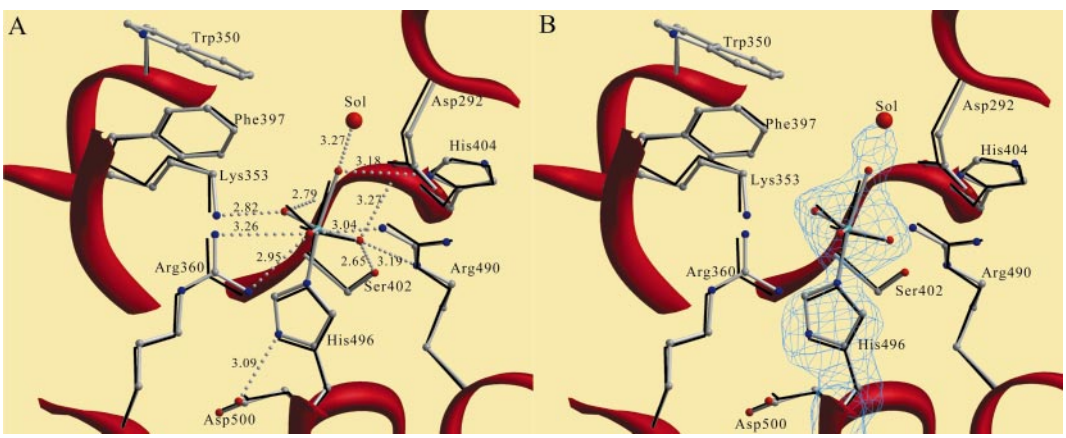

Table 3 Possible hydrogen bonding interactions involving residues in the active site of recombinant chloroperoxidase (HOLO)

Donor (D)	Acceptor (A)	Distance D-A (Å)	Angle D-H-A (°)
Trp350 Nε1	His222 O	3.03	144.8
Lys353 Nζ	Pro398 O	3.01	139.3
Lys353 Nζ	Pro401 O	2.58	118.4
Arg360 Nε	Phe397 O	3.04	158.1
Arg360 Nη1	Val495 O	2.82	158.1
His404 Nε2	Trp289 O	2.81	128.4
His404 Nε2	Ala290 O	2.80	135.3
Ala405 N	Ser402 Oγ	3.13	169.3
His496 Nδ1	Asp500 Oδ2	2.97	153.7
Trp497 N	Asp500 Oδ2	3.01	161.3

As observed in the native structure, the vanadate is held by hydrogen bonds to Lys353 (2.79 Å), Arg360 (3.21 Å) and Ser402 (2.77 Å) side chains, and to the amide groups of residues Gly403 (3.09 Å) and Ala404 (3.07 Å). In addition, two hydrogen bonds are formed between Sol1207 (2.61 Å), Sol1210 (2.53 Å) and the equatorial oxygen OV1. The apical oxygen is hydrogen bonded to Sol1089 (2.68 Å) and to Sol1051 (2.81 Å). The number of hydrogen bonds formed with the bound anion is not strongly reduced when compared with the native enzyme. Thus, the vanadate is strongly bound to the protein as suggested by the relatively low average *B*-value for this anion after refinement (21.6 Å^2). The overall structure of the active site remains virtually unchanged, as expected from the large number of interactions fixing the position of both side chains and the main chain in the anion binding pocket. The movement of the Arg490 side chain seems to be necessary for stabilisation of this H404A mutant. This side chain helps to fix the conformation of the loop containing residues Trp289 and Ala290. Maintaining the conformation of this region is probably very relevant for the folding and stability of V-CPO. The removal of the His404 side chain nearly completely abolishes the chlorinating activity of the chloroperoxidase. The activity of this mutant is less than 0.1% of the holoenzyme produced recombinantly (HOLO), suggesting the importance of this residue for catalysis. It is unclear, however, whether this loss of activity is a direct result of the removal of His404 or from the structural changes in the active site that are accompanied by this mutation.

D292A

The residue Asp292 is located close to the vanadate binding site and forms a strong salt bridge with Arg490. This salt bridge helps to orient the side chain of Arg490 for optimal hydrogen bonding with the bound vanadate. When the Asp292 is mutated to an Ala, the conformation of the active site remains unchanged (Fig. 7). The carboxyl group of the Asp292 is replaced by a solvent molecule which hydrogen bonds to the side chain of Arg490. Although the salt bridge is destroyed, the conformation of Arg490 is almost unaltered and seems to be fixed simply by the interaction with internal solvent molecules (Sol1115 and Sol1197). The active site vanadium is covalently bound to His496 (1.97 Å), to three equatorial oxygen ligands (1.60 Å) and to an apical oxygen (2.20 Å) which could constitute a water ligand [28–32]. The bound vanadate is held by hydrogen bonds to the side chains of Lys353 (2.91 Å), Arg360 (2.97 and 3.26 Å), Ser402 (2.74 Å), Arg490 (3.11 and

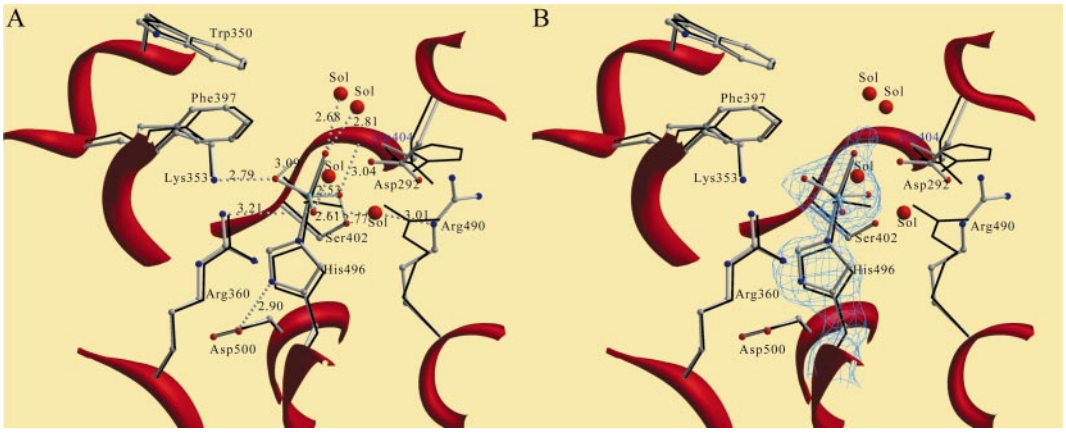

Fig. 6A,B Active site view of mutant H404A. The vanadate is displayed as a *ball and stick model* with oxygens in *red* and the vanadium atom in *blue*. For comparison the conformation of the same residues in the native protein [13] is displayed in *black*. Part of the main chain is represented as a *red ribbon*. **A** The hydrogen bonds are represented as *grey spheres* and the distances are indicated in Å. **B** The electron density map contoured at 4σ was calculated after omitting His496 and the bound vanadate

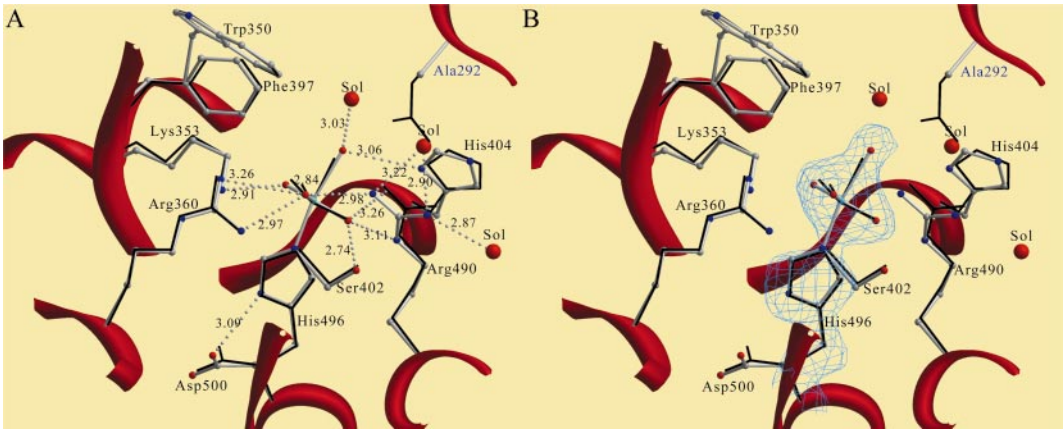

Fig. 7A,B Active site view of mutant D292A. The vanadate is displayed as a *ball and stick model* with oxygens in *red* and the vanadium atom in *blue*. Part of the main chain is represented as a *red ribbon*. For comparison the conformation of the same residues in the native protein [13] is displayed in *black*. **A** The hydrogen bonds are represented as *grey spheres* and the distances are indicated in Å. **B** The electron density map contoured at 4σ was calculated after omitting His496 and the bound vanadate

2.98 Å) and to the amide groups of Gly403 (2.84 Å) and His404 (3.26 Å). The side chain His404 Nδ1 is 3.06 Å away from the apical oxygen of the vanadate ion. This apical oxygen is hydrogen bonded to Sol1053 (3.03 Å).

The active site vanadate ion is strongly held in the active site by a large number of hydrogen bonds. This explains the very low average *B*-value calculated for this oxyanion (16.19 Å^2). From the analysis of this structure we could expect this D292A mutant to display some peroxidase activity. Still, a closer analysis of the electrostatic potential distribution in the proximity of the active site for this mutant reveals that removal of the negative charge creates a strongly positive (blue colour in Fig. 3D) electrostatic potential in the proximity of the active site. This is increased by the above-described movement of the region 390–396, which brings the side chain of Lys394 to the proximity of the active site channel. This side chain makes a strong hydrogen bond to the carbonyl of Ala292. The combination of the mutation and the movement of the Lys394 side chain cause an alteration of the electrostatic potential in the vicinity of the active site channel. Activity measurements under standard chloroperoxidase assay conditions revealed a large decrease in chlorinating activity in this mutant (2% of that of the recombinant holoenzyme). It remains to be determined whether this large reduction in the activity is the result of the change in the electrostatic potential or from a direct role of Asp292 in the catalytic mechanism of the enzyme.

H496A

Upon removal of the His496 side chain a vanadate ion is still found at the active site of the enzyme. Because a covalent bond is no longer formed, the vanadate is found in a tetrahedral conformation, with three non-protein oxygen ligands at a distance of 1.56 Å, and one non-protein oxygen ligand at a distance of 1.67 Å.

At the active site of the H496A mutant (Fig. 8) the tetrahedral vanadate is found forming hydrogen bonds to the side chains of Lys353 (2.76 Å), Arg360 (2.89 and 3.06 Å), Ser402 (2.84 Å), Arg490 (3.14 and 2.96 Å), to the main chain amide groups of Gly403 (2.95 Å) and His404 (3.18 Å) and to solvent molecule Sol219 (2.98 and 2.66 Å). The apical oxygen of the vanadate ion forms a hydrogen bond with the side chain of His404 (3.01 Å) and with Sol1002 (2.54 Å). Most of the side chains at the active site remain in a conformation very similar to their conformation in the native enzyme. The empty space left by removal of the His side chain is filled up by new solvent molecules which interact with the vanadate and help fix the conformation of residues in the active site such as Asp500 (2.72 Å). Since the covalent bond between the vanadate and the protein is missing, this anion is much more loosely bound to the active site of the enzyme as seen from the relatively high average *B*-value it displays (37.50 Å^2). This mutant does not exhibit any haloperoxidase activity. The binding of the vanadate(V) with the covalent bond between the vanadium and the Nε2 of His496 could be necessary for the formation of the monoperoxo-vanadium(V) complex intermediate as observed in the crystal structure of the CPO-peroxo complex [13].

R360A

The residue Arg360 is involved in the compensation of the negative charge of the metal cofactor. In the native enzyme the conformation of the side chain of this residue seems to be optimised for the interaction with the vanadate. The position of the side chain is stabilised by the formation of hydrogen bonds with the carbonyl groups of Phe397 and Val495, residues located at the metal binding site.

The metal in the R360A mutant is found covalently bound to His496 (2.01 Å), to three equatorial non-protein oxygen atoms (1.58–1.62 Å) and to an apical hy-

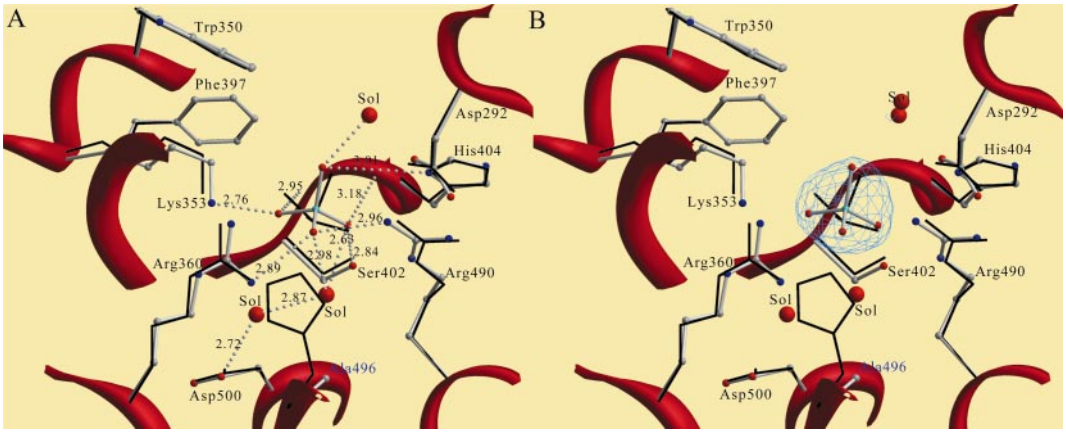

Fig. 8A,B Active site view of mutant H496A. The vanadate is displayed as a *ball and stick model* with oxygens in *red* and the vanadium atom in *blue*. Part of the main chain is represented as a *red ribbon*. For comparison the conformation of the same residues in the native protein [13] is displayed in *black*. **A** The hydrogen bonds are represented as *grey spheres* and the distances are indicated in Å. **B** The electron density map contoured at 4σ was calculated after omitting the vanadate

droxide group (1.77 Å [32]). The hydrogen vanadate is then held by a number of hydrogen bonds (Fig. 9) to the side chains of Lys353 (2.83 Å), Ser402 (2.52 Å), His404 (3.18 Å) and Arg490 (3.22 and 2.77 Å) and to the main chain nitrogens of Gly403 (2.81 Å) and His404 (3.17 Å). The apical hydroxyl ligand is forming an additional hydrogen bond to Sol1193 (2.55 Å), and one of the equatorial oxygens (OV1), which was originally hydrogen bonded to Arg360 in the native protein, is now hydrogen bonded to a new solvent molecule (Sol1217, 2.53 Å). Curiously, the side chain of Lys394 moves in order to replace the hydrogen bond Arg360 was making with Phe397O. This side chain is fixed by an additional hydrogen bond with the new water molecule. As observed for mutant H404A, it seems to be necessary for the enzyme to fulfill some of the hydrogen bonding potential of the residues forming the metal binding site. This could be necessary for the enzyme to maintain the integrity and overall stability around the active site.

Activity measurements, under standard conditions for chlorination, reveal residual activity for this mutant (6% of that of the recombinant holoenzyme), which might be predicted from the structure. Interestingly, preliminary analysis of the kinetic parameters shows increased K_m values for the substrates, showing that this residue affects the activity but is not essential. A detailed kinetic analysis of this mutant (together with the mutants R490A and K353A) will be reported elsewhere.

Conclusions

The active site of V-CPO forms a very rigid matrix designed for oxyanion binding. This rigidity results from the large number of hydrogen bonding interactions involving both the side chains and the main chain of the residues providing this oxyanion binding frame. The presence of a significant number of positively charged residues in this frame provides favourable electrostatic

Fig. 9A,B Active site view of mutant R360A. The vanadate is displayed as a *ball and stick model* with oxygens in *red* and the vanadium atom in *blue*. Part of the main chain is represented as a *red ribbon*. For comparison the conformation of the same residues in the native protein [13] is displayed in *black*. **A** The hydrogen bonds are represented as *grey spheres* and the distances are indicated in Å. **B** The electron density map contoured at 4σ was calculated after omitting His496 and the vanadate

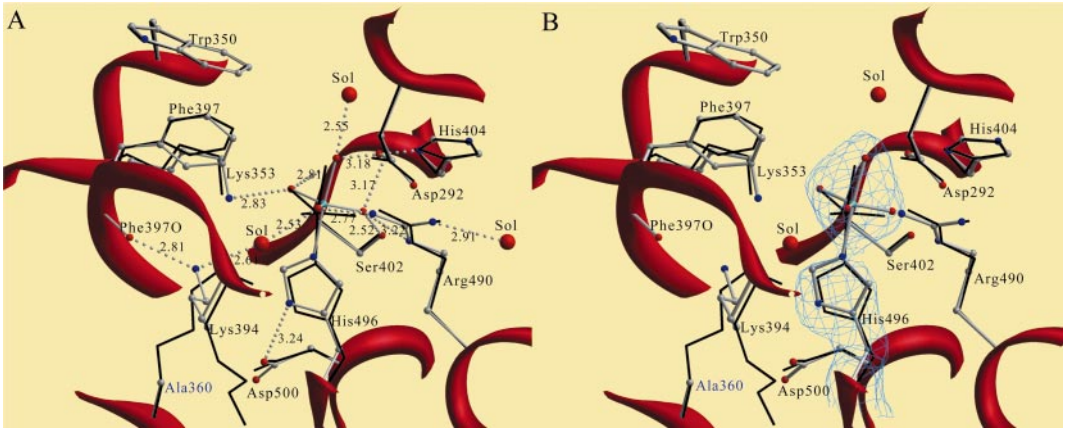

interactions with the negatively charged oxyanions. Thus this site has relative affinities for $HVO_4^{2-} > HPO_2^{2-} > SO_2^{2-}$ (data not shown), binds tungstate and we could predict it to bind molybdate, as was shown for the vanadium bromoperoxidase [34]. The differences in affinities for these oxyanions could result first from the possibilities they have to form a covalent bond with the active site His496, and additionally from the distribution of hydrogen bond donors in the protein in correlation with the protonation state of the oxyanion. Thus, this active site is optimised for the stabilisation of the binding of a tetrahedral oxyanion. We could expect the phosphate to bind in a similar way to the sulfate but with stronger interactions. Additional groups attached to the phosphate in the phosphatase substrates could also play a role in determination of active site affinities.

The rigidity of this active site frame is also observed when the residues which constitute the active site are mutated to alanines. In general, no large shifts of the remaining side or main chains occur and the empty space left by removal of the large side chains is usually occupied by additional solvent molecules. Those solvent molecules also replace some of the hydrogen bonding interactions disrupted by the absence of the mutated residues, maintaining the conformation of the vanadate and of other side chains. It seems that the side chains directly interacting with the vanadate are positioned in optimal conformation through a number of hydrogen bonds with residues forming this metal binding site. As observed from the structure of the CPO mutants, it can be concluded that maintaining the conformation of the active site is much more complex than could be expected and does not depend solely on the optimisation of the interactions with the oxyanion metal group. Instead, the large number of hydrogen bonds observed in the metal binding site seem to act synergistically, favouring the interactions with the vanadate and additionally maintaining the overall stability of this region. Thus, in the mutant H404A we could observe the movement of the Arg490 side chain towards the carbonyls of Ala290 and Trp298, at the expense of breaking a strong salt bridge with Asp292 and, most surprisingly, loosening the interactions to the metal cofactor.

Acknowledgments We thank Prof. R. Huber for supporting this project and for all the valuable suggestions. W.R., R.R. and R.W. thank the Netherlands Foundation for Chemical Research (SON), the Netherlands Organisation for Scientific Research (NOW) and the Netherlands Technology Foundation (STW) for financial support. S.M.-R. has a fellowship PraxisXXI/BD/4050/94 from Fundação para a Ciência e Tecnologia (FCT, Portugal).

References

1. Wiesner W, Van Pée KH, Lingens F (1988) J Biol Chem 263:13725–13732
2. Hofmann B, Tolzer S, Pelletier I, Altenbuchner J, Van Peé KH, Hecht HJ (1998) J Mol Biol 279:889–900
3. Hager LP, Morris DR, Brown FS, Eberwein H (1966) J Biol Chem 241:1769–1777
4. Zeng J, Fenna RE (1992) J Mol Biol 226:185–207
5. De Boer E, Van Kooyk Y, Tromp MGM., Plat H, Wever R (1986) Biochim Biophys Acta 869:48–53
6. Plat H, Krenn BE, Wever R (1987) Biochem J 248:277–279
7. Vilter H (1984) Phytochemistry 23:1387–1390
8. Vilter H (1995) In: Sigel HS, Sigel A (eds) Metals ions in biological chemistry, vol. 31. Dekker, New York, pp 326–362
9. Vollenbroek EG, Simons LH, van Schijndel JW, Barnett P, Balzar M, Dekker H, van der Linden C, Wever R (1995) Biochem Soc Trans 23:267–271
10. Van Schijndel JWPM, Vollenbroek EJM, Wever R (1993) Biochim Biophys Acta 1161:249–256
11. Barnett P, Kruitbosch DL, Hemrika W, Dekker HL, Wever R (1997) Biochim Biophys Acta 1352:73–84
12. Messerschmidt A, Wever R (1996) Proc Natl Acad Sci USA 93:392–396
13. Messerschmidt A, Prade L, Wever R (1997) Biol Chem 378:309–315
14. Van Schijndel JWPM, Barnett P, Roelse J, Vollenbroek EGM, Wever R (1994) Eur J Biochem 225:151–157
15. Hemrika W, Renirie R, Dekker HL, Barnett P, Wever R (1997) Proc Natl Acad Sci USA 94:2145–2149
16. Neuwald AF (1997) Protein Sci 6:1764–1767
17. Leslie A (1991) In: Moras D, Podjarny AD, Thierry JC (eds) Crystallographic computing V. Oxford University Press, Oxford, pp 27–38
18. Collaborative Computational Project No. 4 (1994) Acta Crystallogr D50:760–763
19. Navaza J (1994) Acta Crystallogr A50:157–163
20. Brünger GJ (1993) XPLOR (version 3.1). A system for X-ray crystallography and NMR. Yale University Press, New Haven
21. Engh R, Huber R (1991) Acta Crystallogr A47:392–400
22. Roussel A, Cambillau C (1989) TurboFRODO in Silicon Graphics geometry. Partners Directory, Silicon Graphics, Mountain View, Calif
23. Dauter Z, Sieker LC, Wilson KS (1992) Acta Crystallogr B48:42–59
24. McDonald IK, Thornton JM (1994) J Mol Biol 238:777–793
25. Evans SV (1990) J Mol Graphics 11:134–138
26. Nicholls A, Bharadwaj R, Honig B (1993) Biophys J 64:A166
27. Messerschmidt A, Wever R (1998) Inorg Chim Acta 273:160–166
28. Mimoun H, Saussine L, Daire E, Postel M, Fischer J, Weiss R (1983) J Am Chem Soc 105:3101–3110
29. Zah-Letho J, Samuel E, Dromzee Y, Jeannin Y (1987) Inorg Chim Acta 126:35–38
30. Drew RE, Einstein FWD (1973) Inorg Chem 12:829–835
31. Ogino H, Shimoi M, Saito Y (1989) Inorg Chem 28:3596–3600
32. Kojima A, Okazaki K, Ooi S, Saito K (1983) Inorg Chem 22:1168–1174
33. Aschwanden S, Schmalle HW, Reller A, Oswald HR (1993) Mater Res Bull 28:575–590
34. De Boer E, Boon K, Wever R (1988) Biochemistry 27:1629–1635